ACS APPLIED MATERIALS & INTERFACES

Research Article

www.acsami.org

Facile and Scalable Fabrication of Highly Efficient Lead Iodide Perovskite Thin-Film Solar Cells in Air Using Gas Pump Method

Bin Ding,[†] Lili Gao,[†] Lusheng Liang,[‡] Qianqian Chu,[†] Xiaoxuan Song,[†] Yan Li,[†] Guanjun Yang,*[,†] Bin Fan,[‡] Mingkui Wang,[§] Chengxin Li,[†] and Changjiu Li[†]

[†]State Key Laboratory for Mechanical Behavior of Materials, School of Materials Science & Engineering, Xi'an Jiaotong University, Xi'an, 710049, People's Republic of China

[‡]Weihua Solar Co. Ltd., Xiamen, 361115, People's Republic of China

[§]Wuhan National Laboratory for Optoelectronics, School of Optical and Electronic Information, Huazhong University of Science and Technology, Luoyu Road 1037, Wuhan, 430074, People's Republic of China

S *Supporting Information*

ABSTRACT: Control of the perovskite film formation process to produce high-quality organic−inorganic metal halide perovskite thin films with uniform morphology, high surface coverage, and minimum pinholes is of great importance to highly efficient solar cells. Herein, we report on large-area light-absorbing perovskite films fabrication with a new facile and scalable gas pump method. By decreasing the total pressure in the evaporation environment, the gas pump method can significantly enhance the solvent evaporation rate by 8 times faster and thereby produce an extremely dense, uniform, and full-coverage perovskite thin film. The resulting planar perovskite solar cells can achieve an impressive power conversion efficiency up to 19.00% with an average efficiency of 17.38 ± 0.70% for 32 devices with an area of 5 × 2 mm, 13.91% for devices with a large area up to 1.13 cm^2. The perovskite films can be easily fabricated in air conditions with a relative humidity of 45−55%, which definitely has a promising prospect in industrial application of large-area perovskite solar panels.

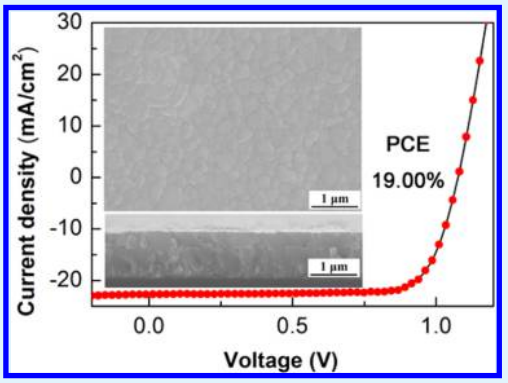

KEYWORDS: *facile, scalable, gas pump, highly efficient, perovskite, solar cell*

INTRODUCTION

Since $CH_3NH_3PbI_3$ was first reported as a sensitizer for solar cell applications in 2009,[1] the development of perovskite solar cells has accelerated dramatically. Several investigations have confirmed that organometallic halide perovskite materials ($CH_3NH_3PbX_3$, where X = Cl, Br, or I) acting as light harvesters[2,3] have long electron−hole diffusion lengths.[4−10] The efficiency of perovskite cells has rapidly increased in recent years. To date, the highest efficiency reported for perovskite-based solar cells is 22% on a rigid substrate[11] and ∼15% on flexible substrates.[12] However, these high efficiencies were achieved in devices with areas less than a square centimeter. It remains challenging to assemble highly efficient large-sized perovskite solar cells containing several functional layers, typically those for electron transport, light absorption, and hole transport. These complex systems require the deposition of dense, uniform, and full-coverage perovskite films without pinholes over large areas.[13] Scientists have typically created perovskite films using either solution[14−17] or vacuum vapor[18,19] deposition processes. The widely used solution-processable one-step deposition method can produce perovskite films with the desired chemical compositions. However, the method creates films with the fatal disadvantage of poor coverage, inevitably containing voids or pinholes.[20] A two-step method of coating PbI_2 solution directly onto a blocking layer and then dipping substrates into a CH_3NH_3I solution has permitted the formation of high-coverage perovskite films to assemble highly efficient devices. However, problems remain in this method, such as rough surfaces,[21] unreacted CH_3NH_3I or PbI_2,[22,23] and the peeling and dissolution of the PbI_2 film during the dipping in CH_3NH_3I solution.[24] Thus, several investigators have recently attempted to ameliorate the one-step method to achieve high-quality scalable perovskite layer fabrication.[25−29] Different approaches have been suggested, but nearly all require time-consuming heat treatment procedures at up to 100 °C to remove solvents. Such heating may cause a number of problems, such as the formation of pinholes in perovskite film, as the direct contact between the hole transport materials and the compact layer will accelerate the recombination of charge carriers.

Here, we report our findings on a facile gas pump (GP) perovskite film fabrication method based on a pressure-induced

Received: May 17, 2016
Accepted: July 18, 2016
Published: July 18, 2016

DOI: 10.1021/acsami.6b05862
ACS Appl. Mater. Interfaces 2016, 8, 20067−20073

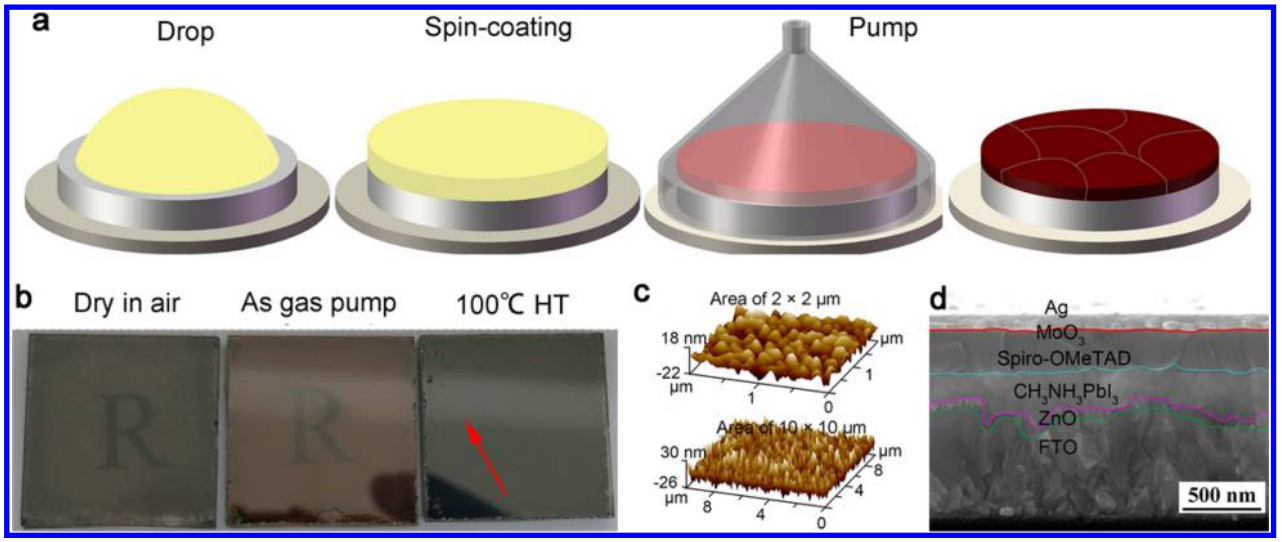

Figure 1. (a) Fabrication process of perovskite films based on the GP method. (b) Photographs of perovskite films made by conventional air-drying and by the GP method with and without HT. (c) Three-dimensional AFM images of small area (2 × 2 μm) and large area (10 × 10 μm). (d) Cross-sectional view of the tested perovskite solar cells using active layers fabricated by the GP method.

gas flow mechanism, which produces extremely dense, uniform, and full-coverage perovskite thin films in less than 20 s at room temperature. By decreasing the total pressure in the evaporation environment, the DMF evaporation rate is significantly accelerated, resulting in a homogeneous precipitation distribution of the solute (i.e., perovskite), and, therefore, a homogeneous perovskite film, on the substrate surface. Because the evaporation of solvents is accelerated, perovskite crystals can be formed on most substrates, including heat-sensitive polymer substrates for applications as flexible photovoltaics.

EXPERIMENTAL SECTION

Materials. CH_3NH_3I and PbI_2 were purchased from Weihua Solar Company. Other materials were purchased from either Alfa Aesar or Sigma-Aldrich.

Fabrication of the Solar Cells. FTO glass substrates with the sheet resistance of 10 Ω sq^{-1} were first cut by laser and then washed by ultrasonication with acetone, ethanol, and deionized water for 10 min each. An 80 nm thick ZnO layer was sputtered onto the clean FTO glass substrates by ion-sputtering. The substrates were treated in a UV/O_3 cleaner machine for 15 min. PbI_2 was mixed with CH_3NH_3I in the molar ratio of 1:1 in *N*,*N*-dimethylformamide (DMF) heated to 70 °C with stirring for 3 h to produce a 40 wt % $CH_3NH_3PbI_3$ solution. The $CH_3NH_3PbI_3$ solution was spun onto the ZnO-coated substrate at 3000 rpm for 10 s. Then, the substrate was put into a sample chamber connecting to gas pump system. The system was home-developed, composed of the low pressure system with a larger low pressure chamber being connected to the sample chamber by a gas drainage pipe controlled by a valve. By opening the valve connecting the specimen chamber and the low pressure system maintaining at 100 Pa, fast pumping of the sample chamber leads to rapid evaporation of DMF solvent. Within 20 s after beginning pumping the gas, a brown, somewhat transparent, film with a mirror-like surface was obtained. For the conventional spin-coating method, the as-spun perovskite wet film was put in dry air for 5 min. The film was annealed at 100 °C on a hot plate for 10 min, and then transferred into a glovebox containing < 0.1 ppm of O_2 and H_2O. A spiro-OMeTAD solution (400 mg of spiro-OMeTAD, 142.5 μL of 4-*tert*-butylpyridine, and 87.5 μL of lithium-bis(trifluoromethanesulfonyl)imide dissolved in 5 mL of chlorobenzene) was deposited onto the perovskite films by spin-coating at 3000 rpm for 30 s. The spiro-OMeTAD-coated substrates were stored in an auto-drying cabinet at 20 °C with a relative humidity of 15% for 8 h. Finally, a 10 nm thick MoO_3 layer and a 120 nm thick Ag layer were deposited onto the spiro-OMeTAD layer by thermal evaporation. The perovskite films were completed in a cleanroom where the temperature was 23 °C and the relative humidity was ~45−55%.

Characterization. In order to measure the phase composition of the perovskite film obtained by the GP method, XRD (D8 Advance, Bruker) was applied with a scanning range of 10−70° and a scanning speed of 0.05°/s. The top-view and cross-view morphologies of the perovskite film were observed by field-emission SEM (MIRA3, TESCAN). The roughness of the perovskite films was measured by atomic force microscopy (Innova, Bruker). Photocurrent−voltage (*J*−*V*) characteristics of the devices were measured by applying a source meter (2400, Keithley) under 100 mW/cm^2 illumination by a 450 W Class AAA solar simulator equipped with an AM 1.5G filter (Sol3A, Oriel). The exact light intensity was determined by a standard Si reference cell (91150V, Oriel). The devices were measured by reverse (1.2 to −0.2 V) and forward (−0.2 to 1.2 V) voltage scanning at a scan step of about 23.7 mV (60 points in total) and a delay time of 100 ms. PL spectroscopy was performed using a compact steady-state spectrophotometer (Fluoromax-4, Horiba Jobin Yvon) with an excitation wavelength of 560 nm. The absorption spectra of the perovskite film were measured with a U-3010 spectrophotometer. The EQE was measured using a solar cell spectral response/QE/IPCE test system (QTest Station 500AD, CROWNTECH) in AC mode. To investigate the electrochemical properties of the perovskite solar cell, we used electrochemical impedance spectroscopy (EIS, Zennium IM6, Zahner), obtained at a bias potential equal to the open-circuit voltage, which was measured at a light intensity of 100 mW/cm^2. The spectra were scanned at a frequency ranging from 4 MHz to 5 Hz with an AC amplitude of 20 mV.

RESULTS AND DISCUSSION

Figure 1a depicts the schematics of the preparation of perovskite films by the GP method. First, 40 wt % $CH_3NH_3PbI_3$ precursor solution was spun on fluorine-doped tin oxide (FTO)/glass substrates coated with a dense ZnO blocking layer, which is known to be higher electron mobility than that of TiO_2, relatively lower cost, simpler deposition process, and prepared at low temperature.[14,30,31] Here, the ZnO compacet layer was prepared by ion-beam sputtering deposition. The substrates are then placed in a sample chamber connecting to a GP system via a gas drainage pipe controlled by a valve. We found that the pressure should be lower than the

DOI: 10.1021/acsami.6b05862
ACS Appl. Mater. Interfaces 2016, 8, 20067−20073

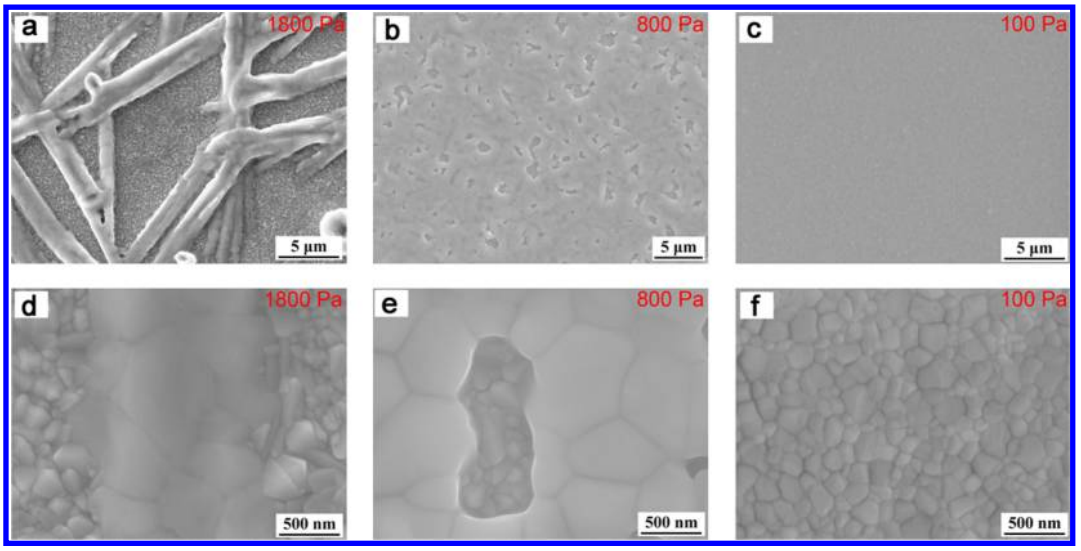

Figure 2. Surface morphologies of $CH_3NH_3PbI_3$ films obtained by GP method. Low- and high-magnification SEM images of perovskite films obtained by GP method at different pressures: (a, d) 1800 Pa, (b, e) 800 Pa, and (c, f) 100 Pa.

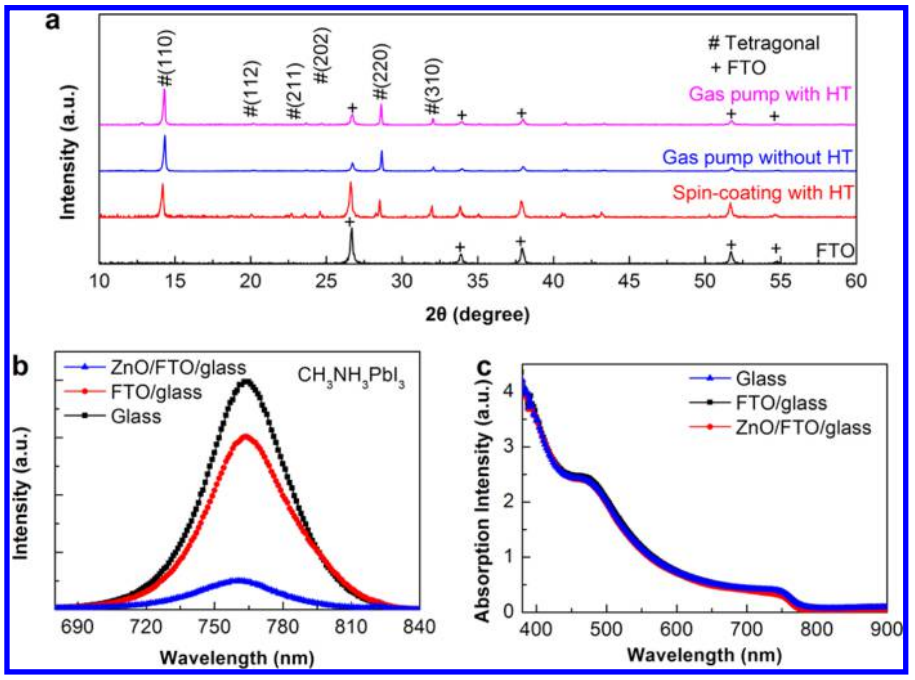

Figure 3. (a) The XRD patterns of FTO substrate and $CH_3NH_3PbI_3$ films fabricated by conventional spin-coating (with air-drying) and GP method. (b) PL emission spectra of $CH_3NH_3PbI_3$ in contact with different interfaces: glass, FTO, and ZnO. (c) The absorption spectra of $CH_3NH_3PbI_3$ in contact with different interfaces: glass, FTO, and ZnO.

saturated vapor pressure of DMF throughout the evaporation process. By establishing a low pressure of 100 Pa, the evaporation of DMF solvent occurs rapidly. A brown perovskite film can be formed in 20 s. The color of the film darkens after heat treatment (HT) at 100 °C for 10 min. Figure 1b compares optical images of perovskite films fabricated by a conventional spin-coating and drying method, the GP method without HT, and the GP method with HT. The perovskite film prepared by the GP process is smooth with an optical mirroring effect (reflecting lamp as shown by the red arrow). Meanwhile, the film fabricated by the conventional spin-coating method is gray and rough with no mirroring.[32] Atomic force microscopy (AFM) characterization under tapping mode was performed to further investigate the surface morphology of the perovskite film prepared by the GP method. Figure 1c shows the corresponding three-dimensional surface profile of the GP perovskite film. The root-mean-square of surface roughness (RMS) is estimated as 7.9 nm in a 10 × 10 μm area and 6.0 nm in a 2 × 2 μm area. This equals one of the best values reported for perovskite films of 2 × 2 μm in area obtained by the solvent−solvent extraction method.[33] The device architecture of the perovskite solar cells in this study is FTO/ZnO-CL/$CH_3NH_3PbI_3$/spiro-OMeTAD/MoO_3/Ag as shown in Figure 1d. This depicts an SEM image of one of the perovskite devices used in this study, containing an ∼80 nm ZnO compact layer, ∼300 nm GP-processed $CH_3NH_3PbI_3$ layer, ∼250 nm spiro-OMeTAD layer, ∼10 nm MoO_3 layer, and ∼120 nm Ag layer.

DOI: 10.1021/acsami.6b05862
ACS Appl. Mater. Interfaces 2016, 8, 20067−20073

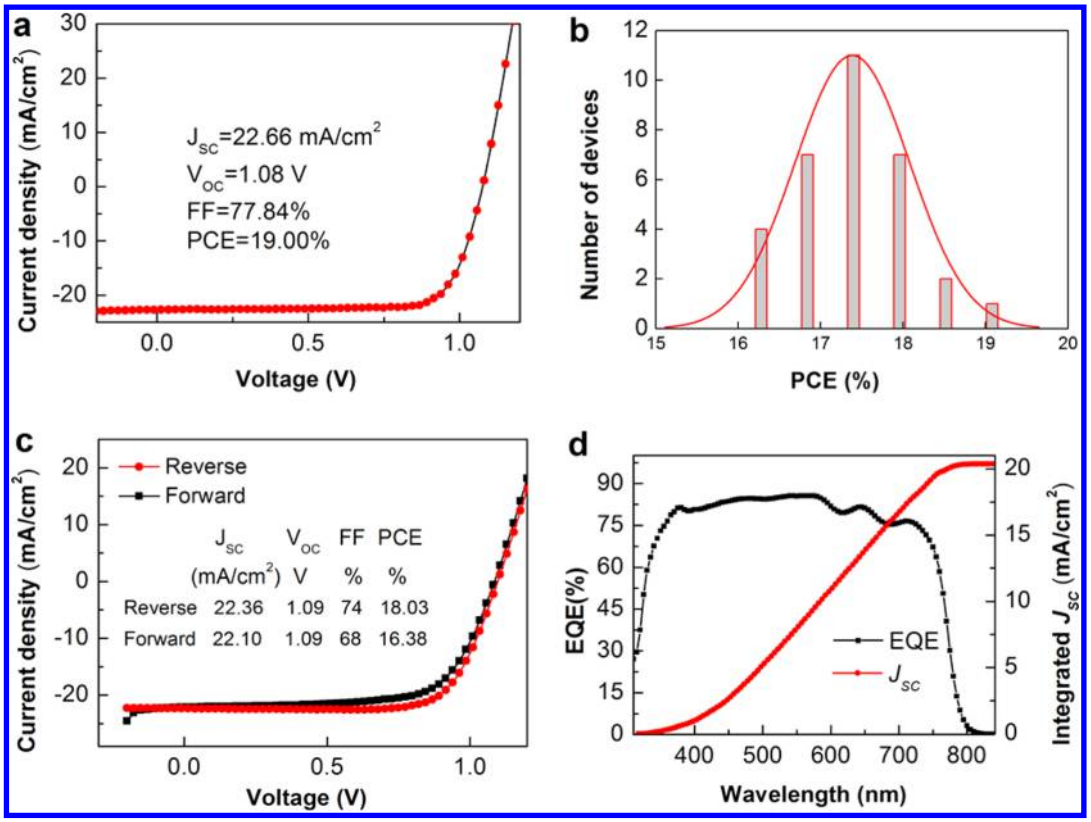

Figure 4. (a) $J-V$ characteristics for the best device. (b) Histogram of power conversion efficiency for 32 devices prepared by the GP method. (c) Typical $J-V$ curve obtained by reverse and forward scans for the device at a scan step of 23.7 mV and delay time of 1000 ms. (d) The corresponding EQE spectrum together with integrated J_{SC} for the device in (c).

The perovskite film dried in air shows the rod-shaped top structure with a large bottom perovskite grain inlaid in the rod and small perovskite grains also deposited on the substrate (Figure S1).[34] To solve this problem, people achieved uniform perovskite films by fast crystallization of perovskite, introducing $PbCl_2$ nuclei,[34] or gas-assisted method.[28] In this study, we achieved fast crystallization of perovskite by accelerating the evaporation of the solvent. To accelerate the evaporation of the solvent, decreasing the atmospheric pressure is an effective approach. Figure 2a,d shows the morphologies of perovskite films made by the GP method in which the ambient pressure is reduced to 1800 Pa and depicts a perovskite film with poor coverage but also a few, and thereby large, grains together with very small grains. On the basis of these observations, faster evaporation of the solvent by further reducing the pressure was necessary. A pressure of 800 Pa was attempted (Figure 2b,e). The coverage of perovskite film is obviously increased, but some of the FTO substrate remains uncovered. When the pressure is reduced to 100 Pa, we obtained uniform, dense, and full-coverage perovskite films with uniform grain size (Figure 2c,f). In this case, the DMF solvent can evaporate very fast since the chamber pressure of 100 Pa is lower than the saturated partial vapor pressure of DMF at room temperature is about 490 Pa.[35] Therefore, the wet perovskite film can be completely dried within 20s, which is much shorter than the general several minutes in conventional ambient drying methods.

Figure 3a presents the X-ray diffraction (XRD) patterns of various $CH_3NH_3PbI_3$ films deposited onto FTO substrates. The sharp diffraction peaks correspond well to the (110), (112), (211), (202), (220), and (310) crystal planes, indicating that the perovskite films are tetragonal in phase with high crystallinity.[36] The diffraction peaks of the FTO substrate appear in the XRD patterns of all three perovskite films, but with different relative intensities, indicating that the perovskite films obtained by the GP method have higher coverage than those made by conventional spin-coating and air-drying. In addition, this result reveals that the tetragonal phase of $CH_3NH_3PbI_3$ exists stably in films prepared by the GP process at room temperature without HT at 100 °C. When in contact with charge-transport layers, perovskite films typically exhibit strong photoluminescence (PL) quenching as evidence of efficient charge transfer from the photoactive to transport layers.[37] Figure 3b shows the steady-state PL spectra of perovskite/glass, perovskite/FTO/glass, and perovskite/ZnO/FTO/glass. Clear quenching of PL emissions can be observed in the spectrum of the sample containing the ZnO compact layer. This indicates that charge carriers within the perovskite layer are extracted effectively by metal oxides such as ZnO.[37,38] We also measured the absorption spectra of $CH_3NH_3PbI_3$ in contact with different interfaces: glass, FTO, and ZnO. Figure 3c shows that the absorption intensity of perovskite films by the gas pump method on different substrates was comparative, indicating that our ZnO film on the FTO substrate can hardly influence the absorption of perovskite films.

Perovskite solar cells were further fabricated using the GP fabricated films by standard procedures. Table S1 shows photovoltaic parameters of perovskite solar cells for using perovskite films fabricated in dry air and by the gas pump method in pressures of 1800, 800, and 100 Pa, indicating that the devices perform badly with extremely low efficiency using perovskite films prepared in dry air. While using the gas pump

DOI: 10.1021/acsami.6b05862
ACS Appl. Mater. Interfaces 2016, 8, 20067−20073

method, the efficiency increases with decreasing the pressure, for the coverage of perovskite film increasing in Figure 2. On the basis of the gas pump method in a pressure of 100 Pa, the best efficiency up to 19.00% was achieved for a perovskite solar cell with a short-circuit current J_{SC} of 22.66 mA/cm^2, the open-circuit voltage V_{OC} of 1.08 V, and a fill factor FF of 0.7784. Figure 4b shows the corresponding $J-V$ curve of such a device. Besides, we achieved device performance of an average efficiency of 17.38 ± 0.70% (Figure 4b for 32 devices) and good reproducible photovoltaic parameters (Figure S2a,c,b). The high efficiency could be attributed to two factors. The first is a uniform, dense, and pinhole-free perovskite film, since direct contact between the hole transport materials and the compact layer at pinholes in the perovskite film would accelerate the recombination of charge carriers. The second is the good crystallinity and large crystal size of the perovskite film. Larger crystal sizes, here of ∼0.2−0.4 μm as shown in Figure 2f, are reported to increase the photovoltaic performance of crystalline films by reducing the number of grain boundaries and thereby reducing charge recombination.[39] Hysteresis is a controversial issue in perovskite solar cells. Many reports suggest that hysteresis originates from the weak bonding interface between the perovskite film and substrate surface.[40] The device was measured by reverse and forward scans at a scan step of 23.7 mV and delay time of 40, 100, 500, and 1000 ms as shown in Figure S3. With increasing scan delay time, the efficiency is larger and the hysteresis is smaller, but the photocurrent density is smaller. Figure 4c shows the $J-V$ curve with different scanning directions (reverse and forward) with the average efficiency of 17.21% at a scan delay time of 1000 ms. A small hysteresis is observed, which could be attributed to the large crystalline grains with fewer grain boundaries. Figure 4d shows the external quantum efficiency (EQE) of the device in Figure 4c, with an integrated J_{SC} of 20.37 mA/cm^2, which is a little smaller than that obtained from the $J-V$ curve. The absorption band reaching ∼800 nm is consistent with the reported literature data for the light-harvesting ability of $CH_3NH_3PbI_3$ perovskite.[22,41] In order to investigate the internal charge carrier transportation and recombination occurring in the device based on the gas pump method and the air-drying method, electronic impedance spectroscopy (EIS) measurements were performed from 4 MHz to 5 Hz at V_{OC} under illumination by a monochromatic light source. Two frequency-dependent elements are easily observed from the obtained Nyquist plots (Figure S2d). In the order of increasing frequency, these elements are attributed to charge carrier recombination at the interfaces between the perovskite and charge extraction layers, and to charge transfer at the counter electrode together with transport through the hole conductor.[42,43] The EIS data are fitted by an RC circuit,[42,43] as shown in the inset of Figure S2d; the low charge transfer resistance (R1, ∼20 Ω for air-drying method and ∼26 Ω for gas pump method) indicates efficient charge extraction in this device based on both the air-drying method and the gas pump method. However, the high interfacial charge recombination resistance (R2, ∼278 Ω for air-drying method and ∼604 Ω for gas pump method) indicates a much lower recombination in devices based on the gas pump method.

We quantitatively evaluated the evaporation rate of the DMF solvent by comparing a $CH_3NH_3PbI_3$ solution dried in air to that dried by the GP process at room temperature. The evaporated volume of DMF solvent was 4.8 mL for the GP method and 0.6 mL for that in air after the same period of 4 h (Figure 5a). This indicates that the evaporation rate of the DMF solvent in the GP method is 8 times higher than that in conventional air-drying. With this fast evaporation, the precipitation of solid perovskite grows into grains with larger sizes of ∼300 nm that fully cover the substrate surface. To further demonstrate large-area solar cell fabrication, we prepared a device measuring 2.05 × 0.55 cm. Figure 5b shows the $J-V$ curve of this device, with the relatively high efficiency of 13.91%. This result indicates that the facile GP process can be applied to fabricate large-area perovskite solar cells.

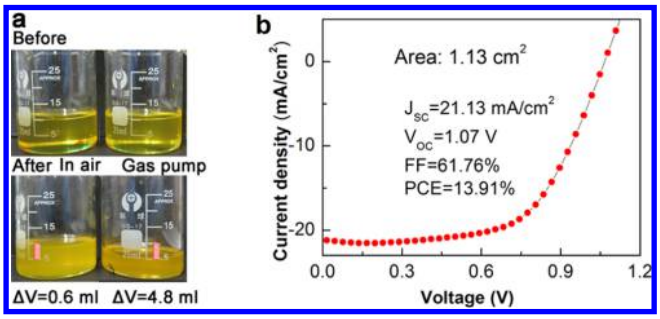

Figure 5. (a) Quantitative comparison of DMF solvent evaporation rate of perovskite solution for 4 h by conventional air-drying versus GP method. (b) $J-V$ curve of a 2.05 × 0.55 cm large-area device containing GP-processed perovskite film at a simulated AM 1.5G solar illumination of 100 mW/cm^2.

CONCLUSIONS

In conclusion, we achieved dense, uniform, and full-coverage perovskite thin film by fast crystallization. On the basis of this, we adopted low pressure evaporation of solvent to achieve fast crystallization of perovskite. Experiments indicate that the evaporation rate of the DMF solvent based on low pressure is 8 times higher than that based on the conventional method. We report on large-area light-absorbing perovskite films fabrication with a new facile and scalable gas pump method. Planar perovskite solar cells can achieve an impressive power conversion efficiency up to 19.00% with an average efficiency of 17.38 ± 0.70% for devices with an area of 5 × 2 mm, 13.91% for devices with a large area up to 1.13 cm^2. We believe that the GP process can be used broadly in the industrial application of perovskite solar cells and other solution-processable thin-film photovoltaics.

ASSOCIATED CONTENT

Supporting Information

The Supporting Information is available free of charge on the ACS Publications website at DOI: 10.1021/acsami.6b05862.

The SEM images of perovskite films dried in air, histograms of photovoltaic parameters, EIS data, typical $J-V$ curves obtained by reverse and forward scan for the device at different scan rates and photovoltaic parameters of perovskite solar cells based on perovskite films fabricated in dry air and by the gas pump method in different pressures (PDF)

AUTHOR INFORMATION

Corresponding Author

*E-mail: ygj@mail.xjtu.edu.cn.

DOI: 10.1021/acsami.6b05862
ACS Appl. Mater. Interfaces 2016, 8, 20067−20073

Notes

The authors declare no competing financial interest.

■ ACKNOWLEDGMENTS

The authors acknowledge financial support from the National Program for Support of Top-notch Young Professionals. We thank Mrs. Nan Zhu, Mr. Bin Xia, and Dr. Xingtian Yin for the AFM, PL, absorption spectra and EQE testing.

■ REFERENCES

(1) Kojima, A.; Teshima, K.; Shirai, Y.; Miyasaka, T. Organometal Halide Perovskites as Visible-Light Sensitizers for Photovoltaic Cells. *J. Am. Chem. Soc.* **2009**, *131*, 6050−6051.

(2) Kim, H. S.; Mora-Sero, I.; Gonzalez-Pedro, V.; Fabregat-Santiago, F.; Juarez-Perez, E. J.; Park, N.-G.; Bisquert, J. Mechanism of Carrier Accumulation in Perovskite Thin-Absorber Solar Cells. *Nat. Commun.* **2013**, *4*, 2242.

(3) Noh, J. H.; Im, S. H.; Heo, J. H.; Mandal, T. N.; Seok, S. I. Chemical Management for Colorful, Efficient, and Stable Inorganic-Organic Hybrid Nanostructured Solar Cells. *Nano Lett.* **2013**, *13*, 1764−1769.

(4) Stranks, S. D.; Eperon, G. E.; Grancini, G.; Menelaou, C.; Alcocer, M. J. P.; Leijtens, T.; Herz, L. M.; Petrozza, A.; Snaith, H. J. Electron-Hole Diffusion Lengths Exceeding 1 Micrometer in an Organometal Trihalide Perovskite Absorber. *Science* **2013**, *342* (6156), 341−344.

(5) Edri, E.; Kirmayer, S.; Mukhopadhyay, S.; Gartsman, K.; Hodes, G.; Cahen, D. Elucidating the Charge Carrier Aeparation and Working Mechanism of $CH_3NH_3PbI_{(3-x)}Cl_{(x)}$ Perovskite Solar Cells. *Nat. Commun.* **2014**, *5*, 3461.

(6) Bai, S.; Wu, Z.; Wu, X.; Jin, Y.; Zhao, N.; Chen, Z.; Mei, Q.; Wang, X.; Ye, Z.; Song, T.; Liu, R.; Lee, S.-t.; Sun, B. High-Performance Planar Heterojunction Perovskite Solar Cells: Preserving Long Charge Carrier Diffusion Lengths and Interfacial Engineering. *Nano Res.* **2014**, *7*, 1749−1758.

(7) Edri, E.; Kirmayer, S.; Henning, A.; Mukhopadhyay, S.; Gartsman, K.; Rosenwaks, Y.; Hodes, G.; Cahen, D. Why Lead Methylammonium Tri-Iodide Perovskite-Based Solar Cells Require a Mesoporous Electron Transporting Scaffold (but not Necessarily a Hole Conductor). *Nano Lett.* **2014**, *14*, 1000−1004.

(8) Dong, Q. F.; Fang, Y. J.; Shao, Y. C.; Mulligan, P.; Qiu, J.; Cao, L.; Huang, J. S. Electron-Hole Diffusion Lengths > 175 μm in Solution-Grown $CH_3NH_3PbI_3$ Single Crystals. *Science* **2015**, *347* (6225), 967−970.

(9) Ball, J. M.; Lee, M. M.; Hey, A.; Snaith, H. J. Low-Temperature Processed Meso-Superstructured to Thin-Film Perovskite Solar Cells. *Energy Environ. Sci.* **2013**, *6*, 1739−1743.

(10) Zhou, H.; Chen, Q.; Li, G.; Luo, S.; Song, T.-b.; Duan, H.-S.; Hong, Z.; You, J.; Liu, Y.; Yang, Y. Interface Engineering of Highly Efficient Perovskite Solar Cells. *Science* **2014**, *345* (6196), 542−546.

(11) National Renewable Energy Laboratory Home Page. http://www.nrel.gov/ (accessed Apr 21, 2016).

(12) Shin, S. S.; Yang, W. S.; Noh, J. H.; Suk, J. H.; Jeon, N. J.; Park, J. H.; Kim, J. S.; Seong, W. M.; Seok, S. I. High-Performance Flexible Perovskite Solar Cells Exploiting Zn_2SnO_4 Prepared in Solution Below 100 Degrees °C. *Nat. Commun.* **2015**, *6*, 7410.

(13) Stranks, S. D.; Snaith, H. J. Metal-Halide Perovskites for Photovoltaic and Light-Emitting Devices. *Nat. Nanotechnol.* **2015**, *10*, 391−402.

(14) Liu, D.; Kelly, T. L. Perovskite Solar Cells with a Planar Heterojunction Structure Prepared Using Room-Temperature Solution Processing Techniques. *Nat. Photonics* **2014**, *8*, 133−138.

(15) Eperon, G. E.; Burlakov, V. M.; Goriely, A.; Snaith, H. J. Neutral Color Semitransparent Microstructured Perovskite Solar Cells. *ACS Nano* **2014**, *8*, 591−598.

(16) Bi, D. Q.; El-Zohry, A. M.; Hagfeldt, A.; Boschloo, G. Improved Morphology Control Using a Modified Two-Step Method for Efficient Perovskite Solar Cells. *ACS Appl. Mater. Interfaces* **2014**, *6*, 18751−18757.

(17) Yang, W. S.; Noh, J. H.; Jeon, N. J.; Kim, Y. C.; Ryu, S.; Seo, J.; Seok, S. I. High-Performance Photovoltaic Perovskite Layers Fabricated Through Intramolecular Exchange. *Science* **2015**, *348* (6240), 1234−1237.

(18) Chen, C. W.; Kang, H. W.; Hsiao, S. Y.; Yang, P. F.; Chiang, K. M.; Lin, H. W. Efficient and Uniform Planar-Type Perovskite Solar Cells by Simple Sequential Vacuum Deposition. *Adv. Mater.* **2014**, *26*, 6647−6652.

(19) Xu, H.-t.; Wu, Y.-l.; Xu, F.-z.; Zhu, J.-b; Ni, C.-w.; Wang, W.-z.; Hong, F.; Xu, R.; Xu, F.; Huang, J.; Wang, L. Grain Growth Study of Perovskite Thin Films Prepared by Flash Evaporation and Its Effect on Solar Cell Performance. *RSC Adv.* **2016**, *6*, 48851−48857.

(20) Cheng, N.; Liu, P.; Bai, S.-h.; Yu, Z.-h.; Liu, W.; Guo, S.-S.; Zhao, X.-Z. Enhanced Performance in Hole Transport Material Free Perovskite Solar Cells via Morphology Control of PbI_2 Film by Solvent Treament. *J. Power Sources* **2016**, *319*, 111−115.

(21) Du, T.; Wang, N.; Chen, H. J.; Lin, H.; He, H. C. Comparative Study of Vapor- and Solution-Crystallized Perovskite for Planar Heterojunction Solar Cells. *ACS Appl. Mater. Interfaces* **2015**, *7*, 3382−3388.

(22) Burschka, J.; Pellet, N.; Moon, S. J.; Humphry-Baker, R.; Gao, P.; Nazeeruddin, M. K.; Gratzel, M. Sequential Deposition as a Route to High-Performance Perovskite-Sensitized Solar Cells. *Nature* **2013**, *499*, 316−319.

(23) Ke, W.; Fang, G.; Wan, J.; Tao, H.; Liu, Q.; Xiong, L.; Qin, P.; Wang, J.; Lei, H.; Yang, G.; Qin, M.; Zhao, X.; Yan, Y. Efficient Hole-Blocking Layer-Free Planar Halide Perovskite Thin-Film Solar Cells. *Nat. Commun.* **2015**, *6*, 6700.

(24) Boopathi, K. M.; Ramesh, M.; Perumal, P.; Huang, Y.-C.; Tsao, C.-S.; Chen, Y.-F.; Lee, C.-H.; Chu, C.-W. Preparation of Metal Halide Perovskite Solar Cells Through a Liquid Droplet Assisted Method. *J. Mater. Chem. A* **2015**, *3*, 9257−9263.

(25) Jeon, N. J.; Noh, J. H.; Kim, Y. C.; Yang, W. S.; Ryu, S.; Seok, S. I. Solvent Engineering for High-Performance Inorganic-Organic Hybrid Perovskite Solar Cells. *Nat. Mater.* **2014**, *13*, 897−903.

(26) Jeon, N. J.; Noh, J. H.; Yang, W. S.; Kim, Y. C.; Ryu, S.; Seo, J.; Seok, S. I. Compositional Engineering of Perovskite Materials for High-Performance Solar Cells. *Nature* **2015**, *517*, 476−480.

(27) Xiao, M. D.; Huang, F. Z.; Huang, W. C.; Dkhissi, Y.; Zhu, Y.; Etheridge, J.; Gray-Weale, A.; Bach, U.; Cheng, Y. B.; Spiccia, L. A Fast Deposition-Crystallization Procedure for Highly Efficient Lead Iodide Perovskite Thin-Film Solar Cells. *Angew. Chem., Int. Ed.* **2014**, *53*, 9898−9903.

(28) Huang, F. Z.; Dkhissi, Y.; Huang, W. C.; Xiao, M. D.; Benesperi, I.; Rubanov, S.; Zhu, Y.; Lin, X. F.; Jiang, L. C.; Zhou, Y. C.; Gray-Weale, A.; Etheridge, J.; McNeill, C. R.; Caruso, R. A.; Bach, U.; Spiccia, L.; Cheng, Y. B. Gas-Assisted Preparation of Lead Iodide Perovskite Films Consisting of a Monolayer of Single Crystalline Grains for High Efficiency Planar Solar Cells. *Nano Energy* **2014**, *10*, 10−18.

(29) Jeon, Y. J.; Lee, S.; Kang, R.; Kim, J. E.; Yeo, J. S.; Lee, S. H.; Kim, S. S.; Yun, J. M.; Kim, D. Y. Planar Heterojunction Perovskite Solar Cells with Superior Reproducibility. *Sci. Rep.* **2014**, *4*, 6953.

(30) Roldan-Carmona, C.; Malinkiewicz, O.; Soriano, A.; Espallargas, G. M.; Garcia, A.; Reinecke, P.; Kroyer, T.; Dar, M. I.; Nazeeruddin, M. K.; Bolink, H. J. Flexible High Efficiency Perovskite Solar Cells. *Energy Environ. Sci.* **2014**, *7*, 994−997.

(31) Xu, X.; Chen, Q.; Hong, Z.; Zhou, H.; Liu, Z.; Chang, W.-H.; Sun, P.; Chen, H.; Marco, N. D.; Wang, M.; Yang, Y. Working Mechanism for Flexible Perovskite Solar Cells with Simplified Architecture. *Nano Lett.* **2015**, *15*, 6514−6520.

(32) Dkhissi, Y.; Huang, F.; Rubanov, S.; Xiao, M.; Bach, U.; Spiccia, L.; Caruso, R. A.; Cheng, Y.-B. Low Temperature Processing of Flexible Planar Perovskite Solar Cells with Efficiency over 10%. *J. Power Sources* **2015**, *278*, 325−331.

(33) Zhou, Y.; Yang, M.; Wu, W.; Vasiliev, A. L.; Zhu, K.; Padture, N. P. Room-Temperature Crystallization of Hybrid-Perovskite Thin

DOI: 10.1021/acsami.6b05862
ACS Appl. Mater. Interfaces 2016, 8, 20067−20073

Films via Solvent-Solvent Extraction for High-Performance Solar Cells. *J. Mater. Chem. A* **2015**, *3*, 8178−8184.
(34) Yan, K.; Long, M.; Zhang, T.; Wei, Z.; Chen, H.; Yang, S.; Xu, J. Hybrid Halide Perovskite Solar Cell Precursors: Colloidal Chemistry and Coordination Engineering behind Device Processing for High Efficiency. *J. Am. Chem. Soc.* **2015**, *137*, 4460−4468.
(35) Cui, X.-l.; Chen, G.m.; Han, X.-h. Experimental Vapor Pressure Data and a Vapor Pressure Equation for N,N-Dimethylformamide. *J. Chem. Eng. Data* **2006**, *51* (5), 1860−1861.
(36) Hu, M.; Liu, L.; Mei, A.; Yang, Y.; Liu, T.; Han, H. Efficient Hole-Conductor-Free, Fully Printable Mesoscopic Perovskite Solar Cells with a Broad Light Harvester NH_2CH-NH_2PbI_3. *J. Mater. Chem. A* **2014**, *2*, 17115−17121.
(37) You, J.; Meng, L.; Song, T. B.; Guo, T. F.; Yang, Y. M.; Chang, W. H.; Hong, Z.; Chen, H.; Zhou, H.; Chen, Q.; Liu, Y.; De Marco, N.; Yang, Y. Improved Air Stability of Perovskite Solar Cells via Solution-Processed Metal Oxide Transport Layers. *Nat. Nanotechnol.* **2016**, *11*, 75−81.
(38) Docampo, P.; Ball, J. M.; Darwich, M.; Eperon, G. E.; Snaith, H. J. Efficient Organometal Trihalide Perovskite Planar-Heterojunction Solar Cells on Flexible Polymer Substrates. *Nat. Commun.* **2013**, *4*, 2761.
(39) Im, J. H.; Jang, I. H.; Pellet, N.; Gratzel, M.; Park, N. G. Growth of $CH_3NH_3PbI_3$ Cuboids with Controlled Size for High-Efficiency Perovskite Solar Cells. *Nat. Nanotechnol.* **2014**, *9*, 927−932.
(40) Cojocaru, L.; Uchida, S.; Jayaweera, P. V. V; Kaneko, S.; Nakazaki, J.; Kubo, T.; Segawa, H. Origin of the Hysteresis in *I-V* Curves for Planar Structure Perovskite Solar Cells Rationalized with a Surface Boundary-induced Capacitance Model. *Chem. Lett.* **2015**, *44*, 1750−1752.
(41) Ahn, N.; Son, D. Y.; Jang, I. H.; Kang, S. M.; Choi, M.; Park, N. G. Highly Reproducible Perovskite Solar Cells with Average Efficiency of 18.3% and Best Efficiency of 19.7% Fabricated via Lewis Base Adduct of Lead(II) Iodide. *J. Am. Chem. Soc.* **2015**, *137*, 8696−8699.
(42) Yang, M.-J; Guo, R.; Kadel, K.; Liu, Y.-Y; O'Shea, K.; Bone, R.; Wang, X.-W.; He, J.; Li, W.-Z. Improved Charge Transport of Nb-doped TiO_2 Nanorods in Methylammonium Lead Iodide Bromide Perovskite Solar Cells. *J. Mater. Chem. A* **2014**, *2*, 19616−19622.
(43) Li, D.; Cui, J.; Li, H.; Huang, D.; Wang, M.-K.; Shen, Y. Graphene Oxide Modified Hole Transport Layer for $CH_3NH_3PbI_3$ Planar Heterojunction Solar Cells. *Sol. Energy* **2016**, *131*, 176−182.

DOI: 10.1021/acsami.6b05862
ACS Appl. Mater. Interfaces 2016, 8, 20067−20073